

Coupling JOREK and STARWALL Codes for Non-linear Resistive-wall Simulations

M. Hölzl¹, P. Merkel¹, G.T.A. Huysmans², E. Nardon³,
E. Strumberger¹, R. McAdams^{4,5}, I. Chapman⁵, S. Günter¹,
K. Lackner¹

¹Max-Planck-Institute for Plasmaphysics, EURATOM Association, Boltzmannstr. 2, 85748 Garching, Germany

²ITER Organisation, Route de Vinon sur Verdon, St-Paul-lez-Durance, France

³CEA, IRFM, CEA Cadarache, F-13108 St Paul-lez-Durance, France

⁴York Plasma Institute, University of York, York, YO10 5DD, UK

⁵Euratom/CCFE Fusion Association, Culham Science Centre, Abingdon, OX14 3DB, UK

E-mail: mhoelzl@ipp.mpg.de

Abstract. The implementation of a resistive-wall extension to the non-linear MHD-code JOREK via a coupling to the vacuum-field code STARWALL is presented along with first applications and benchmark results. Also, non-linear saturation in the presence of a resistive wall is demonstrated. After completion of the ongoing verification process, this code extension will allow to perform non-linear simulations of MHD instabilities in the presence of three-dimensional resistive walls with holes for limited and X-point plasmas.

1. Introduction

Plasma instabilities growing on fast time-scales such as vertical displacement events, disruptions, external kink modes, or edge localized modes are connected with a time-dependent magnetic perturbation outside the plasma. The mirror currents induced in conducting structures around the plasma¹ by the varying field perturbations act back onto the instabilities. Thus, linear and non-linear dynamics of the plasma can be strongly influenced by the wall. An external kink mode driven by strong edge current densities, for instance, is converted into a resistive wall mode (RWM) in the presence of a conducting wall close to the plasma edge and grows on the timescale of resistive wall-current decay as described in great detail in Refs. [1, 2].

We describe the status of a resistive wall extension for the non-linear MHD code JOREK [3, 4] as well as first benchmark results. The implementation is done by coupling JOREK to a modified version of the STARWALL code [5] which determines the magnetic field in the vacuum region in the presence of three-dimensional walls with holes. The “response” of conducting structures to magnetic field perturbations is represented by response-matrices computed by STARWALL. These matrices are used in JOREK to keep track of wall-currents and calculate the tangential magnetic field required for the modified boundary conditions as discussed in Section 3.2.

The article provides some information about the STARWALL code in Section 2. The coupling equations are derived in Section 3. First benchmarks of the resistive wall extension are presented

¹ For simplicity, all conducting structures are denoted wall in the following.

in Section 4. Conclusions and a brief outlook are given in Section 5.

2. The STARWALL Code

STARWALL solves the vacuum magnetic field equation outside the JOEK computational domain in presence of a three-dimensional conducting wall with holes as a Neumann-like problem. The continuity of the magnetic field component normal to the boundary of the JOEK computational domain (called interface) is used as a boundary condition. The wall is represented by infinitely thin triangles which allows to approximate realistic wall structures very well using an effective resistance η_w/d_w where η_w and d_w denote the resistivity of the wall material² and its thickness, respectively. Wall currents are assumed constant within each triangle such that they can be described by current potentials Y_k at the triangle nodes [5]³.

In case of an ideally conducting wall, solving the vacuum field equation results in an algebraic expression for the magnetic field component tangential to the interface⁴ in terms of the normal component. Wall currents don't need to be considered explicitly as they are instantaneously given by the normal field at the interface. Using the ideal wall response-matrix \hat{M}^{id} calculated by STARWALL, this can be written in the following way⁵:

$$B_{\text{tan}} = \sum_i b_i B_{\text{tan},i} = \sum_i b_i \sum_j \hat{M}_{i,j}^{\text{id}} \Psi_j. \quad (1)$$

Here, b_i denotes a JOEK basis function consisting of a 1D Bezier basis function along the poloidal direction on the interface and Fourier basis function in toroidal direction. Ψ_j denotes poloidal flux coefficients. The poloidal flux at the interface is given by $\Psi = \sum_j b_j \Psi_j$.

When a resistive wall is considered, wall currents cannot be eliminated anymore. In this case, the tangential magnetic field is given by

$$B_{\text{tan}} = \sum_i b_i \left(\sum_j \hat{M}_{i,j}^{\text{ee}} \Psi_j + \sum_k \hat{M}_{i,k}^{\text{ey}} Y_k \right), \quad (2)$$

where wall currents evolve in time according to

$$\dot{Y}_k = -\frac{\eta_w}{d_w} \hat{M}_{k,k}^{\text{yy}} Y_k - \sum_j \hat{M}_{k,j}^{\text{ye}} \dot{\Psi}_j. \quad (3)$$

Here, \hat{M}^{ee} , \hat{M}^{ey} , \hat{M}^{ye} , and \hat{M}^{yy} denote resistive response matrices determined by STARWALL. Indices i and j run over all boundary degrees of freedom of the respective variable and k over all wall current potentials. For cross-checking, a relation between ideal and resistive response matrices can be derived by letting $\eta_w \rightarrow \infty$ (Appendix A).

Information about the STARWALL code coupled with CASTOR (sometimes called STARWALL_C) can be found in Refs. [5, 7]. It is similar to the STARWALL code coupled with JOEK (sometimes called STARWALL_J). An article describing more details is in preparation by the STARWALL author Peter Merkel.

3. Implementation in JOEK

For the coupling of JOEK and STARWALL, Eqs. (2) and (3) are discretized in time as described in Section 3.1. The vacuum response then enters into a natural boundary condition in JOEK as discussed in Section 3.2.

² Wall resistivity is normalized the same way as plasma resistivity (see Ref. [6] for JOEK normalizations).

³ For simplicity, we will (inaccurately) speak about wall currents when wall current potentials are referred to.

⁴ B_{tan} is the component of $(\mathbf{B} - \mathbf{B}_\phi)$ tangential to the interface, where \mathbf{B}_ϕ denotes the toroidal field component.

⁵ For practical reasons, the algebraic expression is written in terms of the poloidal flux Ψ instead of the normal field component (which can be calculated from Ψ , of course).

3.1. Time-Discretization

Equation (2) is evaluated at the new timestep $n + 1$ and discretizations $\Psi^{n+1} = \Psi^n + \delta\Psi^n$ and $Y^{n+1} = Y^n + \delta Y^n$ are used, where superscripts indicate evaluation at the given timestep. The tangential magnetic field is thus given by

$$B_{\text{tan}}^{n+1} = \sum_i b_i \left[\sum_j \hat{M}_{i,j}^{\text{ee}} (\Psi_j^n + \delta\Psi_j^n) + \sum_k \hat{M}_{i,k}^{\text{ey}} (Y_k^n + \delta Y_k^n) \right]. \quad (4)$$

The general time-evolution scheme described in Ref. [8],

$$\left[(1 + \xi) \left(\frac{\partial \mathbf{X}}{\partial \mathbf{u}} \right)^n - \Delta t \theta \left(\frac{\partial \mathbf{Z}}{\partial \mathbf{u}} \right)^n \right] \delta \mathbf{u}^n = \Delta t \mathbf{Z}^n + \xi \left(\frac{\partial \mathbf{X}}{\partial \mathbf{u}} \right)^{n-1} \delta \mathbf{u}^{n-1}, \quad (5)$$

is used for the JOREK equations written in the form $\partial \mathbf{X}(\mathbf{u})/\partial t = \mathbf{Z}(\mathbf{u})$, where \mathbf{u} denotes the vector of JOREK physical variables like temperature or density, \mathbf{X} and \mathbf{Z} the left- respectively right-hand side terms of the time-evolution equations, and θ and ξ are numerical parameters⁶. The same general time-evolution method needs to be applied to the wall-current evolution (Eq. (3)) giving

$$\begin{aligned} & (1 + \xi) \left[\delta Y_k^n + \sum_j \hat{M}_{k,j}^{\text{ye}} \delta \Psi_j^n \right] + \Delta t \theta \frac{\eta_w}{d_w} \hat{M}_{k,k}^{\text{yy}} \delta Y_k^n \\ & = - \Delta t \frac{\eta_w}{d_w} \hat{M}_{k,k}^{\text{yy}} Y_k^n + \xi \left[\delta Y_k^{n-1} + \sum_j \hat{M}_{k,j}^{\text{ye}} \delta \Psi_j^{n-1} \right]. \end{aligned} \quad (6)$$

Terms with δY_k^n are brought to the left hand side. The equation then reads

$$\begin{aligned} & \left(1 + \xi + \Delta t \theta \frac{\eta_w}{d_w} \hat{M}_{k,k}^{\text{yy}} \right) \delta Y_k^n \\ & = - (1 + \xi) \sum_j \hat{M}_{k,j}^{\text{ye}} \delta \Psi_j^n - \Delta t \frac{\eta_w}{d_w} \hat{M}_{k,k}^{\text{yy}} Y_k^n + \xi \delta Y_k^{n-1} + \xi \sum_j \hat{M}_{k,j}^{\text{ye}} \delta \Psi_j^{n-1}. \end{aligned} \quad (7)$$

After solving for δY_k^n , one gets

$$\delta Y_k^n = \sum_j \hat{A}_{k,j} \delta \Psi_j^n + \hat{B}_{k,k} Y_k^n + \hat{C}_{k,k} \delta Y_k^{n-1} + \sum_j \hat{D}_{k,j} \delta \Psi_j^{n-1}, \quad (8)$$

where some of the ‘‘derived response matrices’’

$$\begin{aligned} \hat{S}_{k,k} &= 1 + \xi + \Delta t \theta \frac{\eta_w}{d_w} \hat{M}_{k,k}^{\text{yy}} & \hat{D}_{k,j} &= \xi \hat{M}_{k,j}^{\text{ye}} / \hat{S}_{k,k} & \hat{H}_{i,j} &= \hat{M}_{i,j}^{\text{ee}} \\ \hat{A}_{k,j} &= - (1 + \xi) \hat{M}_{k,j}^{\text{ye}} / \hat{S}_{k,k} & \hat{E}_{i,j} &= \hat{M}_{i,j}^{\text{ee}} + \sum_k \hat{M}_{i,k}^{\text{ey}} \hat{A}_{k,j} & \hat{J}_{i,j} &= \sum_k \hat{M}_{i,k}^{\text{ey}} \hat{D}_{k,j} \\ \hat{B}_{k,k} &= - \Delta t \frac{\eta_w}{d_w} \hat{M}_{k,k}^{\text{yy}} / \hat{S}_{k,k} & \hat{F}_{i,k} &= \hat{M}_{i,k}^{\text{ey}} (1 + \hat{B}_{k,k}) & \hat{K}_{k,l} &= - \Delta t \hat{M}_{k,k}^{\text{yy}} \hat{S}_{l,k} \\ \hat{C}_{k,k} &= \xi / \hat{S}_{k,k} & \hat{G}_{i,k} &= \hat{M}_{i,k}^{\text{ey}} \hat{C}_{k,k} & \hat{L}_{i,l} &= \sum_k \hat{M}_{i,k}^{\text{ey}} \hat{K}_{k,l} \end{aligned} \quad (9)$$

⁶ Parameter values satisfying $\theta - \xi = 0.5$ are required to guarantee second-order accuracy of the time-evolution scheme. For instance, $(\theta = 0.5, \xi = 0)$ corresponds to a linearized Crank-Nicholson scheme and $(\theta = 1, \xi = 0.5)$ to the linearized Gears scheme.

have been used. These matrices are computed at the beginning of a JOEREK simulation from the STARWALL response matrices. They need to be updated if one or more parameters entering the definitions have changed, e.g., Δt , ξ , or η_w . Plugging Eq. (8) into Eq. (4) gives

$$B_{\text{tan}}^{n+1} = \sum_i b_i \left[\sum_j \left(\hat{M}_{i,j}^{\text{ee}} + \sum_k \hat{M}_{i,k}^{\text{ey}} \hat{A}_{k,j} \right) \delta \Psi_j^n + \sum_k \hat{M}_{i,k}^{\text{ey}} \left(1 + \hat{B}_{k,k} \right) Y_k^n \right. \\ \left. + \sum_k \hat{M}_{i,k}^{\text{ey}} \hat{C}_{k,k} \delta Y_k^{n-1} + \sum_j \hat{M}_{i,j}^{\text{ee}} \Psi_j^n + \sum_j \sum_k \hat{M}_{i,k}^{\text{ey}} \hat{D}_{k,j} \delta \Psi_j^{n-1} \right] \quad (10)$$

and, making use of Eq. (9), we get

$$B_{\text{tan}}^{n+1} = \sum_i b_i \left[\sum_j \hat{E}_{i,j} \delta \Psi_j^n + \sum_k \hat{F}_{i,k} Y_k^n + \sum_k \hat{G}_{i,k} \delta Y_k^{n-1} + \sum_j \hat{H}_{i,j} \Psi_j^n + \sum_j \hat{J}_{i,j} \delta \Psi_j^{n-1} \right]. \quad (11)$$

3.2. Boundary Integral

The fixed boundary conditions for poloidal flux and plasma current corresponding to an ideally conducting wall are removed from JOEREK. As a consequence, a boundary integral in the current definition equation resulting from partial integration (which vanishes in fixed-boundary JOEREK) needs to be considered now. It can be written in terms of the tangential magnetic field such that we can insert Eq. (11) as a natural boundary condition. Details are given in the following.

The current definition equation, $j = \Delta^* \Psi$, is written in weak form as

$$\int dV \frac{j_l^*}{R^2} (j - \Delta^* \Psi) = 0. \quad (12)$$

where j_l^* denotes the test-functions taken to be identical with the basis-functions. Using $\Delta^* \Psi \equiv R^2 \nabla \cdot (R^{-2} \nabla \Psi)$, we get

$$\int dV \frac{j_l^*}{R^2} j - \int dV j_l^* \nabla \cdot \left(\frac{1}{R^2} \nabla \Psi \right) = 0, \quad (13)$$

where the second term of the resulting expression can be integrated by parts ($\int dV a \nabla \cdot \mathbf{b} = - \int dV \nabla a \cdot \mathbf{b} + \oint dA a \mathbf{b} \cdot \hat{\mathbf{n}}$) yielding

$$\int dV \frac{j_l^*}{R^2} j + \int dV \frac{1}{R^2} \nabla j_l^* \cdot \nabla \Psi - \oint dA \frac{j_l^*}{R} \underbrace{(\nabla \Psi \cdot \hat{\mathbf{n}}/R)}_{\equiv B_{\text{tan}}} = 0. \quad (14)$$

Here, $\hat{\mathbf{n}}$ denotes the unit vector normal to the interface and the tangential field is identified in the boundary integral (refer to [Appendix B](#) for details). Eq. (11) is inserted into Eq. (14) and after separating implicit and explicit terms, we have derived the form of the current equation implemented in JOEREK,

$$\sum_{i_{\text{elem}}} \int \frac{dV}{R^2} (j_l^* \delta j^n + \nabla j_l^* \cdot \nabla \delta \Psi^n) - \sum_{i_{\text{bnd}}} \oint dA \frac{j_l^*}{R} \sum_i b_i \sum_j \hat{E}_{i,j} \delta \Psi_j^n \\ = - \sum_{i_{\text{elem}}} \int \frac{dV}{R^2} (j_l^* j^n + \nabla j_l^* \cdot \nabla \Psi^n) \\ + \sum_{i_{\text{bnd}}} \oint dA \frac{j_l^*}{R} \sum_i b_i \left[\sum_k \left(\hat{F}_{i,k} Y_k^n + \hat{G}_{i,k} \delta Y_k^{n-1} \right) + \sum_j \left(\hat{H}_{i,j} \Psi_j^n + \hat{J}_{i,j} \delta \Psi_j^{n-1} \right) \right], \quad (15)$$

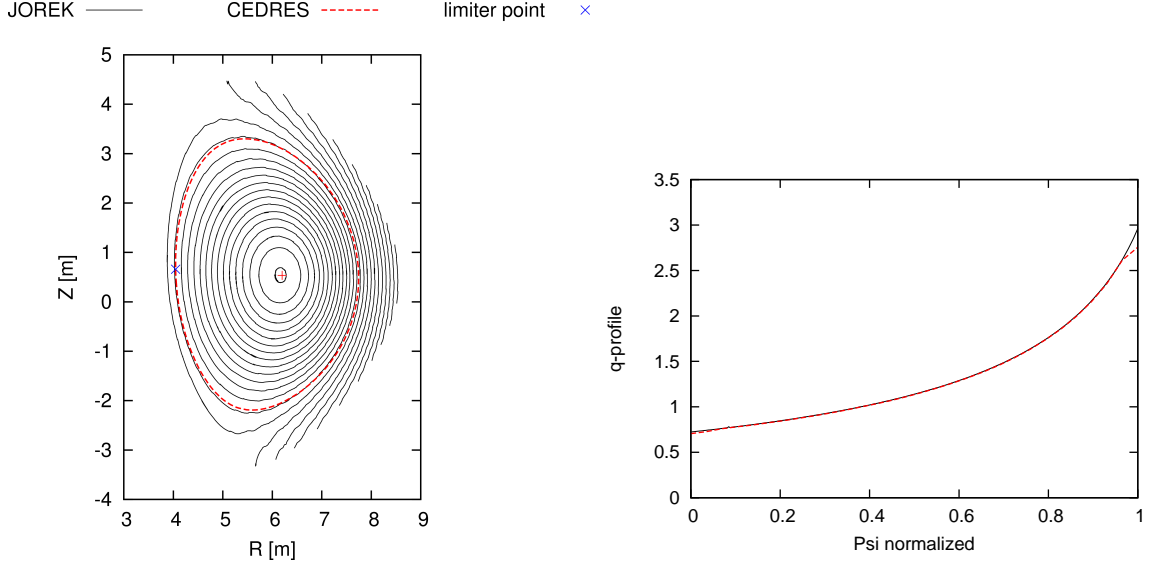


Figure 1

Left: JOREK flux-surfaces of a limiter equilibrium (limiter point shown as blue cross) are compared to CEDRES++ last closed flux-surface and magnetic axis.

Right: Comparison of the respective q -profiles.

with

$$\int dV = \sum_{i_{\text{elem}}} \int du dv d\phi J_2 R, \quad \text{and} \quad \oint dA = \sum_{i_{\text{bnd}}} \int du d\phi R \sqrt{(R_{,u})^2 + (Z_{,u})^2}, \quad (16)$$

where the integral over u and v is carried out by Gauss-quadrature: $\int du X(u) = \sum_{m_G} w_{m_G} X(u_{m_G})$ with weights w_{m_G} and positions u_{m_G} . Coordinate u corresponds to the element-local coordinate of the 2D Bezier elements oriented poloidally along the interface. The other element-local coordinate is denoted v . J_2 denotes the 2D-Jacobian in the poloidal plane. Wall-currents are updated after each time-step according to Eq. (8) to guarantee consistency with the implicit time-stepping of JOREK.

For the $n = 0$ component, poloidal field coils need to be taken into account properly. This is done by replacing the expression for the tangential magnetic field, Eq. (2), by

$$B_{\text{tan}} = \sum_i b_i \left(\sum_j \hat{M}_{i,j}^{\text{ee}} (\Psi_j - \Psi_j^{\text{coil}}) + \sum_k \hat{M}_{i,k}^{\text{ey}} Y_k + B_{\text{tan},i}^{\text{coil}} \right). \quad (17)$$

Here, Ψ_j^{coil} and $B_{\text{tan},i}^{\text{coil}}$ denote time-independent coil contributions to poloidal flux and tangential field at the interface, respectively. This leads to two additional terms in Eq. (15). A similar boundary integral also occurs in the Grad-Shafranov equation giving the plasma equilibrium. Here, only the $n = 0$ component needs to be considered (axisymmetric equilibria in JOREK) and no time-discretization is required.

4. First Benchmarks and Results

In this Section, we present first results of the ongoing benchmark effort for code validation.

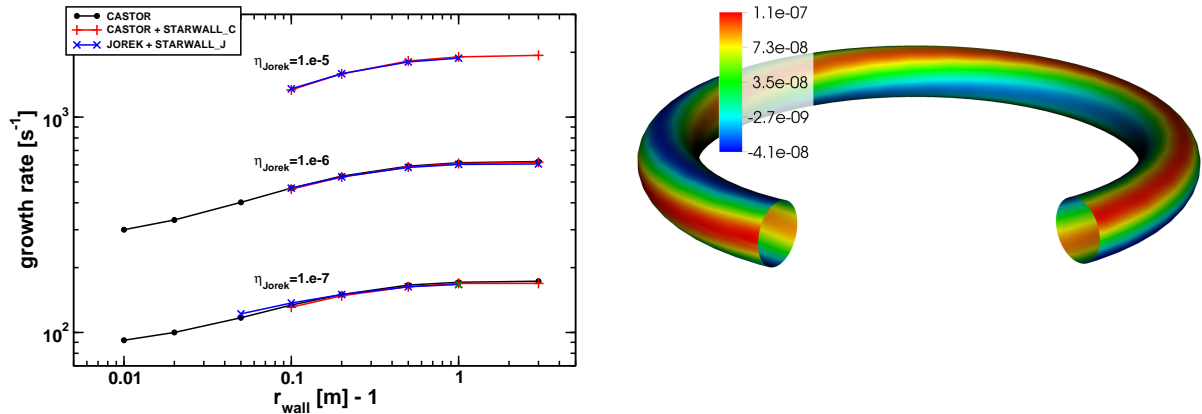


Figure 2

Left: Linear growth-rates of a tearing-mode in a circular plasma with concentric ideal wall are compared between CASTOR using its own vacuum field module, CASTOR coupled with STARWALL, and JOREK coupled with STARWALL. Very good agreement is observed for a variety of different plasma resistivities and plasma-wall distances.

Right: The current potential distribution (arbitrary units) reflecting the 2/1 tearing mode structure is plotted during the linear phase ($\eta_{\text{Jorek}} = 1 \cdot 10^{-6}$, $r_w = 1.2$).

4.1. Free-boundary equilibrium

Computing a free-boundary equilibrium with JOREK and comparing it to the results of another equilibrium solver allows to check some parts specific for $n = 0$ like poloidal field-coil contributions (see Sec. 3.2). We are considering an ITER-like limiter plasma. As seen from Figure 1, flux surfaces and q -profile of the JOREK equilibrium agree very well with the equilibrium computed by the CEDRES++ code [9]. Slightly different discretizations of the poloidal field coils might be responsible for small remaining differences.

4.2. Tearing Mode

A 2/1 tearing mode in a circular plasma with major radius $R = 10$, minor radius $a = 1$ and uniform plasma resistivity surrounded by an ideally conducting wall is considered. Figure 2 shows excellent agreement between JOREK and the linear CASTOR code [10]. Repeating the simulation for a resistive wall with zero resistivity is physically identical, of course, but numerically treated in a different way. The exact agreement we get here proves consistency.

4.3. Resistive Wall Mode

In this Section, results for 2/1 resistive wall modes (RWMs) in a circular plasma with minor radius $a = 1$ and major radius $R = 10$ surrounded by a resistive wall are presented. The left part of Figure 3 shows linear growth rates obtained for different wall radii r_w as a function of the wall resistivity. Clearly, the modes cannot be stabilized beyond a certain wall distance from the plasma even at very low wall resistivities. The right part of the Figure shows energy time-traces during the linear and saturation phase of a typical simulation.

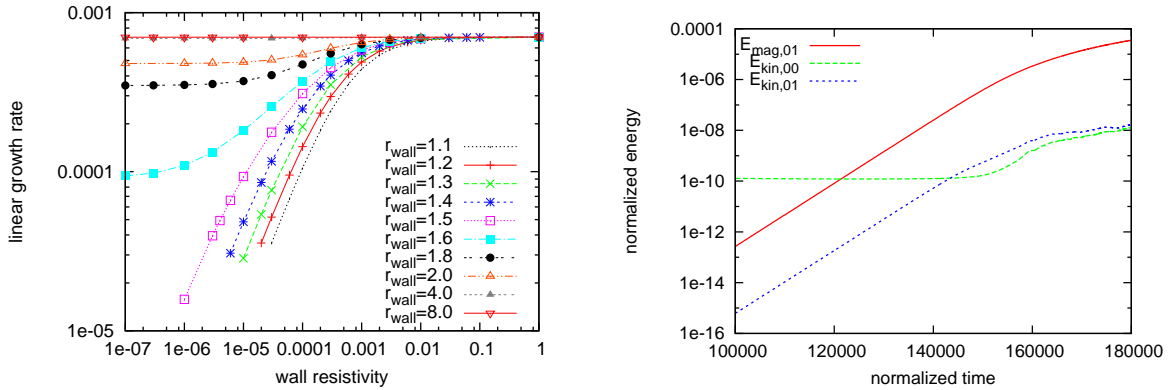


Figure 3

Left: Linear RWM growth rates extracted from the simulations are shown for a variety of wall radii and wall resistivities.

Right: Energy time-traces are shown for linear and saturation phase of an RWM ($r_w = 1.2$, $\eta_{\text{wall}} = 1 \cdot 10^{-4}$). In saturation, wall currents on the high-field side have an amplitude comparable to the low-field side while they are smaller in the linear phase.

5. Conclusions and Outlook

The ongoing implementation and verification of a resistive wall model in the non-linear MHD-code JOREK was summarized. Benchmarks for a freeboundary equilibrium and tearing mode cases show good agreement. Simulations of the linear and non-linear phase of RWMs were presented (comparison to analytical theory and linear codes ongoing).

Benchmarking will be continued and extended to non-linear comparisons. Realistic X-point geometries will be considered requiring a special treatment of grid corners. After completion, the code can be applied to a variety of MHD instabilities interacting with conducting structures like resistive wall modes, edge localized modes, vertical displacement events or disruptions.

Acknowledgements

Simulations were mostly carried out on the HPC-FF computing cluster in Jülich, Germany, and on the IFERC-CSC Helios computing cluster in Rokkasho-Mura, Japan.

References

- [1] Chu M S and Okabayashi M 2010 *Plasma Physics and Controlled Fusion* **52** 123001
- [2] Igochine V 2012 *Nuclear Fusion* **52** 074010
- [3] Czarny O and Huysmans G 2008 *J. Comput. Phys.* **227** 7423 – 7445
- [4] Huysmans G, Pamela S, Beurskens M, Becoulet M and van der Plas E 2010 *Proceedings of the 23rd IAEA Fusion Energy Conference* (Daejeon, South Korea) THS/7-1
- [5] Merkel P and Sempf M 2006 *Proceedings of the 21st IAEA Fusion Energy Conference* (Chengdu, China) TH/P3-8 URL www-naweb.iaea.org/napc/physics/FEC/FEC2006/papers/th_p3-8.pdf
- [6] Hölzl M, Günter S, Wenninger R, Müller W C, Huysmans G, Lackner K, Krebs I and the ASDEX Upgrade Team 2012 *Physics of Plasmas* (accepted)
- [7] Strumberger E, Merkel P, Tichmann C, and Günter S 2011 *Proceedings of the 38th EPS Conference on Plasma Physics* (Strasbourg, France) p5.082 URL <http://ocs.ciemat.es/EPS2011PAP/pdf/P5.082.pdf>
- [8] Hirsch C 1989 *Numerical Computation of Internal and External Flows, Volume 1, Fundamentals of Numerical Discretization* (Wiley) ISBN 978-0-471-92385-5
- [9] Hertout P, Boulbe C, Nardon E, Blum J, Brémond S, Bucalossi J, Faugeras B, Grandgirard V and Moreau P 2011” *Fusion Engineering and Design* **86** 1045–1048 Proceedings of the 26th Symposium of Fusion Technology (SOFT-26)
- [10] Kerner W, Goedbloed J, Huysmans G, Poedts S and Schwarz E 1998 *J. Comput. Phys.* **142** 271 – 303

Appendix A. Relation between ideal and resistive response matrices

Between the ideal and resistive response-matrices, the relation

$$\hat{M}_{i,j}^{\text{id}} \equiv \hat{M}_{i,j}^{\text{ee}} - \sum_k \hat{M}_{i,k}^{\text{ey}} \hat{M}_{k,j}^{\text{ye}} \quad (\text{A.1})$$

must hold which becomes obvious when letting $\eta_w \rightarrow 0$ and inserting Eq. (3) into Eq. (2). Also, the no-wall response can easily be identified as

$$\hat{M}_{i,j}^{\text{nw}} \equiv \hat{M}_{i,j}^{\text{ee}} \quad (\text{A.2})$$

when letting $Y_k \rightarrow 0$. Eqs. (A.1) and (A.2) can be used to cross-check some parts of the implementation as both forms of the wall-treatment with eliminated wall-currents (Eq. (1)) and explicitly treated wall-currents (Eqs. (2) and (3)) are implemented in JOEREK.

Appendix B. Magnetic field tangential to the interface

The magnetic field in the JOEREK reduced-MHD model is given by

$$\mathbf{B} = \frac{F_0}{R} \hat{\mathbf{e}}_\phi + \frac{1}{R} \nabla \Psi \times \hat{\mathbf{e}}_\phi. \quad (\text{B.1})$$

Its component tangential to the boundary of the JOEREK computational domain (in the poloidal plane) can be determined from

$$B_{\text{tan}} = (\mathbf{B} \times \hat{\mathbf{n}}) \cdot \hat{\mathbf{e}}_\phi, \quad (\text{B.2})$$

where $\hat{\mathbf{n}}$ denotes the unit normal vector of the interface and $\hat{\mathbf{e}}_\phi$ the normalized toroidal basis vector. Inserting Eq. (B.1) and using vector identities, this can be written in the form

$$\begin{aligned} B_{\text{tan}} &= -\frac{1}{R} \hat{\mathbf{e}}_\phi \cdot [\hat{\mathbf{n}} \times (\nabla \Psi \times \hat{\mathbf{e}}_\phi)] \\ &= -\frac{1}{R} \hat{\mathbf{e}}_\phi \cdot \left[\underbrace{(\hat{\mathbf{n}} \cdot \hat{\mathbf{e}}_\phi)}_{\equiv 0} \nabla \Psi - (\hat{\mathbf{n}} \cdot \nabla \Psi) \hat{\mathbf{e}}_\phi \right] \\ &= \frac{1}{R} \hat{\mathbf{n}} \cdot \nabla \Psi, \end{aligned} \quad (\text{B.3})$$

which can be identified in the boundary integral of Eq. (14) and replaced by the STARWALL response.